Molecular basis for substrate recognition and septum cleavage by AtlA, the major N-acetylglucosaminidase of Enterococcus faecalis

Véronique Roig-Zamboni, Sarah Barelier, Robert Dixon, Nicola Galley, Amani Ghanem, Quoc Phong Nguyen, Héloize Cahuzac, Bartlomiej Salamaga, Peter Davis, Yves Bourne, et al.

Molecular basis for substrate recognition and septum cleavage by AtlA, the major *N*-acetylglucosaminidase of *Enterococcus faecalis*

Véronique Zamboni [a*], Sarah Barelier[a*], Robert Dixon [b], Nicola Galley [b], Amani Ghanem [a], Phong Nguyen [a], Héloize Cahuzac [b], Bartłomiej Salamaga [b], Peter J. Davis [b], Stéphane Mesnage [b] and Florence Vincent [a]

[a] CNRS, Aix Marseille University, AFMB, Marseille, France

[b] School of Biosciences, University of Sheffield, Sheffield, UK

* These authors contributed equally

Running title: Structure and function of *E. faecalis* glucosaminidase

Keywords: glycosyl hydrolase, structure-function, crystal structure, enterococcus, cell wall, peptidoglycan

Address correspondence to Florence Vincent, fvincent.cnrs@univ-amu.fr or Stéphane Mesnage, s.mesnage@sheffield.ac.uk

Abstract

The cleavage of septal peptidoglycan at the end of cell division leads to the separation of daughter cells. The hydrolases involved in this process (called autolysins) are potentially lethal enzymes that can cause cell death. Their activity must therefore be tightly controlled during cell growth. In *Enterococcus faecalis*, the *N*-acetylglucosaminidase AtlA plays a predominant role in cell separation. *atlA* mutants form long cell chains that can no longer disseminate in the host and are readily taken up by phagocytes. AtlA has structural homologs in other important pathogens such as *Listeria monocytogenes* and *Salmonella typhimurium* and therefore represents an attractive model to design new inhibitors of pathogenesis. Here, we provide a 1.6Å crystal structure of the *E. faecalis* AtlA catalytic domain that reveals a closed conformation of a conserved β-hairpin and a complex network of hydrogen bonds that bring two catalytic residues at an ideal distance for an inverting mechanism. Based on the model of the AtlA-substrate complex, we identify key residues critical for substrate recognition and septum cleavage during bacterial growth.

Introduction

Enterococcus faecalis is a nosocomial pathogen causing a wide range of infections, some of which can be life-threatening (1). The virulence of this organism relies on a combination of several factors acting synergistically to outcompete other organisms and cause the disease. These factors include the capacity to survive abiotic stresses (such as pH changes or exposure to bile salts) and antibiotic treatments (*e.g.*, cephalosporins) (1,2). During pathogenesis, *E. faecalis* has evolved several mechanisms that enable this organism to evade the host innate immune system. These include the production of two distinct cell surface polymers (a capsule and a rhamnopolysaccharide) that play an antiphagocytic role (for review, see (3)). Another mechanism relies on the control of cell chain length. *E. faecalis* has a distinctive morphology and forms diplococci and short cell chains made of 4 to eight cells. The disruption of cell separation at the end of the division, leading to the formation of cell chains, has a dramatic impact on virulence. It prevents the dissemination of bacteria from causing a systemic infection and leads to the uptake of cell chains by phagocytes (4).

One peptidoglycan hydrolase, AtlA, has a predominant role in *E. faecalis* septum cleavage. *atlA* mutants are viable but form extremely long chains and are greatly attenuated in the zebrafish virulence model of infection (4). It has also been shown that AtlA activity contributes to the bactericidal activity of beta-lactam antibiotics (5,6). Based on the contribution of AtlA to pathogenesis and antibiotics-mediated killing, this peptidoglycan hydrolase represents an attractive target to prevent enterococcal infections whilst limiting microbiota changes.

AtlA is a multimodular *N*-acetylglucosaminidase belonging to the glycosyl-hydrolases GH73 family in the CAZY database (7). To avoid AtlA-mediated autolysis, the activity of AtlA is tightly controlled, both spatially and temporally (4). The enzyme undergoes post-translational

modifications (glycosylation and proteolytic cleavage) and preferentially binds to denuded glycan chains (preferentially found at the mid-cell) *via* the C-terminal LysM domain (8).

In this study, we report the first structure that captures a closed conformation of the active site, revealing a single-displacement (inverting) mechanism. We further provide a structure-function analysis of AtlA catalytic domain. We demonstrate the endo-glucosaminidase activity and identify the critical residues for catalysis both *in vitro* and in the context of the live bacteria. Based on these data, we propose a model for the interaction of AtlA with peptidoglycan, a first step towards the rational design of specific inhibitors targeting an enterococcal virulence factor.

Results

Overall Structure of AtlAc

The structure of AtlAc (161 residues) was solved at a resolution of 1.45Å. It adopts a lysozyme α/β fold with an α-lobe containing 5 α-helices (α1: 180-197, α2: 202-213; α3: 265-278, α4: 299-306, α5:315-327), 5 helices 3_{10}, a small β-hairpin (280- 286) and a major β-lobe covering the binding site, made of 2 antiparallel β-strands (β1:239-248, β2: 251-260) connecting α2 and α3 (Figure 1A).

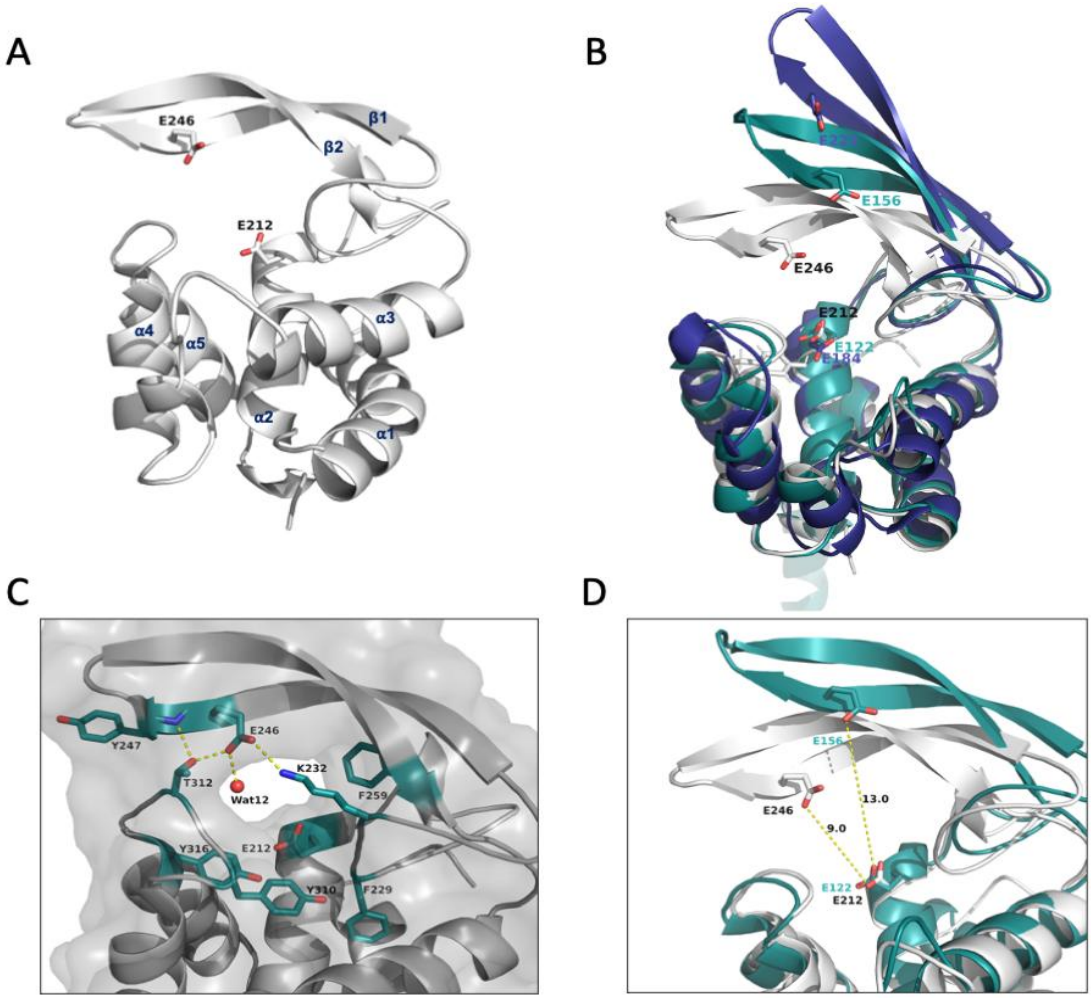

Figure 1: AtlAc structure and overlay of AtlAc, Auto and FlgJ$_{St}$. **A**, Cartoon representation of the structure of AtlAc. The secondary elements are numbered and the catalytic Glu246 and Glu212 are shown in stick. **B,** Overlay of AtlAc in white, Auto from *L. monocytogene* (blue, PDB: 3fi7), and FlgJ from *S. thyphimurium* (FlgJ$_{St}$, Green, PDB 5dn5). The conserved putative

catalytic Glu are shown in stick and colored labels. **C,** Close-up view of AtlAc active site, the conserved residues are shown in blue sticks and hydrogen bonds are illustrated with yellow dashed lines.

This fold superimposes with Auto from *Listeria monocytogenes* with a rmsd of 1.02Å for 107 Cα atoms and with FlgJ from *S. thyphimurium* ($FlgJ_{St}$) with a rmsd of 2.2Å for 119Cα , which account for the larger opening of the β-hairpin (Figure 1B) (9). The structure also contains 5 glycerol molecules coming from the cryogenic conditions. Only one polypeptide of AtlAc is found in the asymmetric unit, suggesting that the protein is monomeric in solution.

The AtlAc active site shows two highly conserved glutamate residues: Glu212 is equivalent to *L. monocytogenes* Auto Glu122 and $FlgJ_{St}$ E184 catalytic residues and is located at a similar position, at the end of helix α1 (Figure 1B). The second predicted catalytic glutamate, Glu246, stands on β2 and is equivalent to Glu156 in *L. monocytogenes* Auto and Glu223 in $FlgJ_{St}$. Unlike Auto and $FlgJ_{St}$ which show an open groove for the active site, the AtlAc active site shapes into a tunnel (Figure 1B and 1D). The β-hairpin closing on the α-lobe by forming several hydrogen bonds: Glu246 OE2 on strand β1 with Lys232 NZ on a loop between α2 and β1, Glu246 with Thr312 OG1 and the water molecule 12 (Wat12), and Thr312 OG1 with Tyr247 main chain N (Figure 1C). Lys232 makes also a bond with OE1 Glu257 on β2, but this Glu residue is not conserved in the GH73 family (Figure 1C and 2).

Several aromatic residues that have been identified in the GH73 family to be essential for substrate binding or catalysis, are also conserved in AtlA active site, namely Tyr310 which belong to the YATD motif, a signature motif of the GH73 family, Tyr316, Phe259 and Phe229 (Figure 1C and 2) (10).

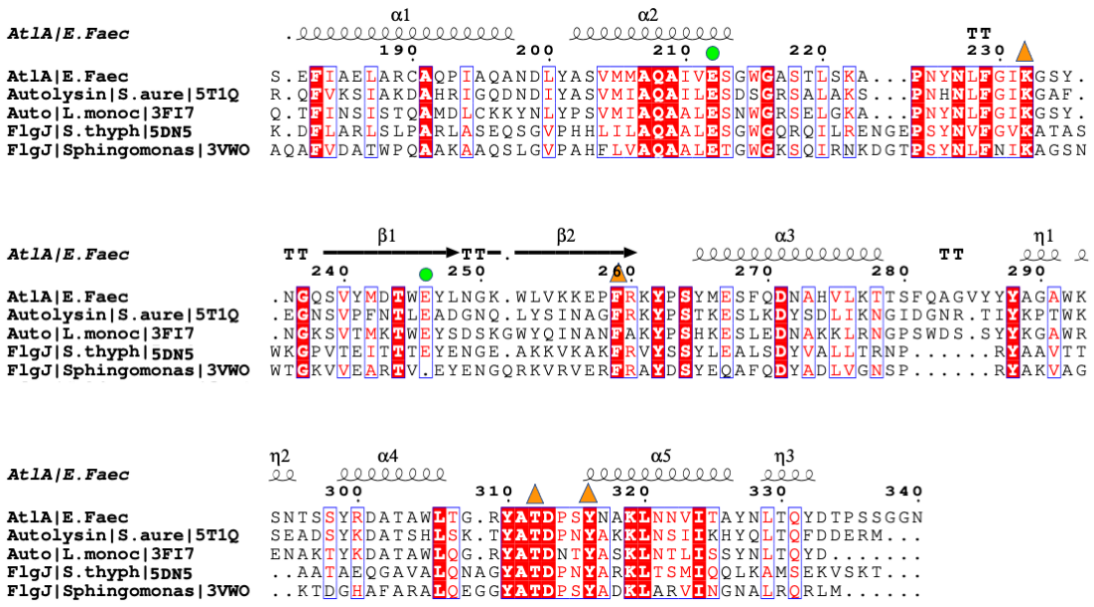

Figure 2: Structure based sequence alignment of several GH73 enzymes. This alignment has been done with the program Expresso (11). AtlAc secondary structures are drawn at the top of the alignment. The conserved putative catalytic glutamate residues are shown with green dots. The mutated residues used in this study are shown with orange triangles.

PG hydrolysis by AtlA

The crystal structure of AtlAc revealed a partial occlusion of the catalytic tunnel by the Lys232 residue (Figure 1C). Based on the analysis of other GH73 catalytic domains, we hypothesized that this residue is flexible to allow the recognition of long glycan chains. An alternative explanation could be that AtlA displays exo-glucosaminidase activity, thereby accommodating a smaller substrate in the catalytic tunnel. To test our hypothesis, we investigated whether AtlA displays exo- or endo-glucosaminidase activity. Purified peptidoglycan sacculi were incubated in the presence of increasing amounts of recombinant AtlA and solubilized muropeptides were analysed by rp-HPLC. We anticipated that an exo-glucosaminidase would release monomeric peptidoglycan fragments, whilst an endo-glucosaminidase activity would release monomeric and multimeric structures simultaneously. The comparison of muropeptide profiles suggested that

AltlA displays endo-glucosaminidase activity as it generated the same proportion of muropeptides with different oligomerization states, irrespective of the amount of enzyme added (Figure 3).

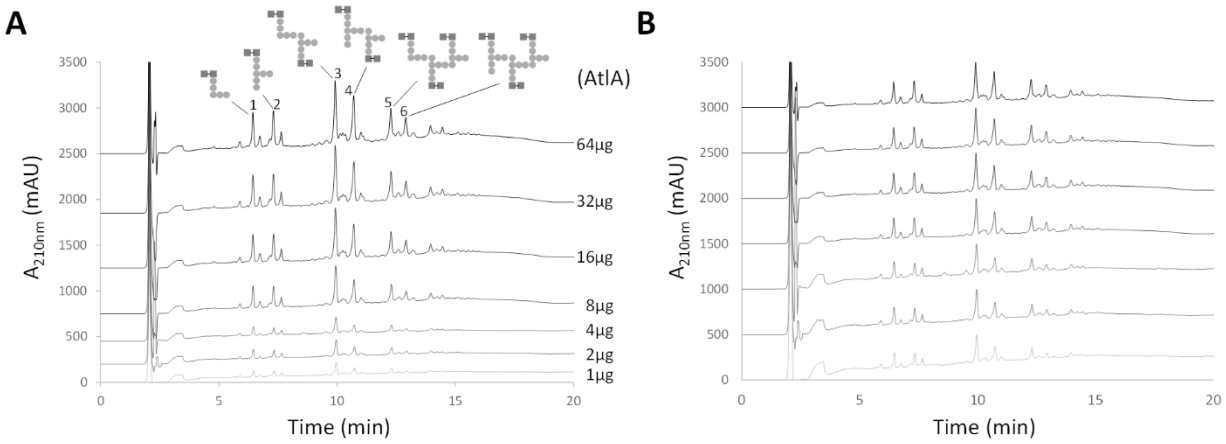

Figure 3. rp-HPLC analysis of muropeptides solubilised by AtlA. A, *E. faecalis* peptidoglycan was digested by increasing amounts of recombinant AtlA (from 1µg to 64µg). Soluble fragments released were reduced and separated on a Hypersil C18 column, showing a mixture of monomers and multimers. The schematic structure of major monomers (peaks 1 and 2), dimers (peaks 3 and 4) and trimers (peaks 5 and 6) is shown. GlcNAc and MurNAc are shown as filled squares, peptide stem residues as filled circles. **B**, All traces were normalised to display the same amplitude for the major dimer, showing no preferential release of monomeric structures and an overall very similar profile, irrespective of the amount of enzyme used.

Docking of a peptidoglycan substrate to the active site of AtlA

To gain insight into AtlA catalytic mechanism and peptidoglycan binding mode, a peptidoglycan fragment was docked to the crystal structure of the enzyme. We used a tetrasaccharide chain ($MurNAc^{-2}$-$GlcNAc^{-1}$-$MurNAc^{+1}$-$GlcNAc^{+2}$) with MurNAc residues substituted by short tripeptide stems found in *E. faecalis* peptidoglycan (L-Ala-γD-Gln-L-Lys) and amenable to docking experiments (Figure S1). The ligand was docked to a grid that encompasses the putative active site of AtlA and includes the two predicted catalytic glutamates, Glu212 and Glu246. The protein was kept rigid except for Lys232, which blocks part of the active site tunnel and has to be

flexible to accommodate the substrate and allow AtlA endo-glucosaminidase activity. The docking produced 8 poses for the ligand with binding energies ranging from −6.5 to −5.4 kcal/mol. Figure 4A shows the docked complex with the ligand in its best (lowest energy) binding pose. Interestingly, docking experiments using peptidoglycan ligands with shorter side chains (L-Ala–D-Gln, or L-Ala) produced the same pose as for the longer side chain (Figure S2). The ligand adopts an extended conformation that spans the active site of AtlA, going through the tunnel that contains the two putative catalytic glutamates. The oxygen of Glu212 is located 2.8 Å away from the glycosidic bond, in agreement with the cleavage of the glycosidic bond between $GlcNAc^{-1}$ and $MurNAc^{+1}$. The ligand mainly interacts via the $GlcNAc^{-1}$ moiety, making several hydrogen bonds with the backbones of Gly230, Trp245, Tyr310, Thr312, Asp313 and with the side chain of Glu246 (Figure 4B), suggesting that the $MurNAc^{+1}$– $GlcNAc^{+2}$ part of the substrate is the first to leave the active site after cleavage. The other sugar moieties of the ligand also establish hydrogen bonds with the protein *via* $MurNAc^{-2}$ (with Tyr310), $MurNAc^{+1}$ (with Glu212) and $GlcNAc^{+2}$ (with Asp243). Although potential interactions may involve the amino acid side chains of the ligands (with residue Val211, for example), the flexibility of the peptide stems renders such predictions unreliable.

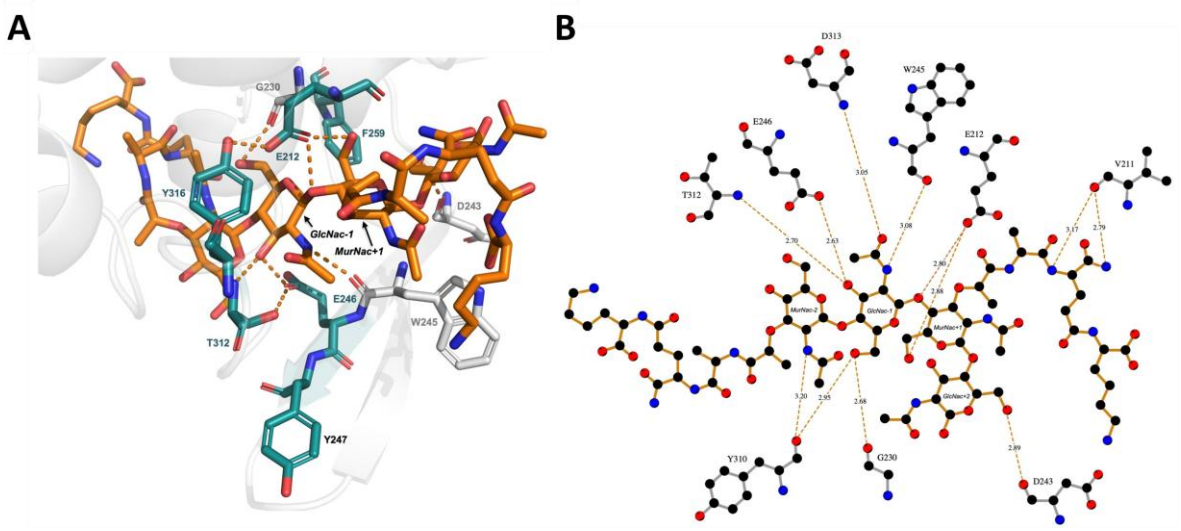

Figure 4. Model of the interaction between a peptidoglycan substrate and Atla. A, Top scoring pose of a peptidoglycan substrate docked to the active site of Atla. The ligand substrate is represented as orange sticks, the receptor is represented as light grey cartoon, the main residues of the active site are shown in sticks and the residues selected for mutational studies are highlighted in blue. **B,** Ligplot+ representation of the interactions of a peptidoglycan substrate (ligand) with the active site residues of Atla (receptor).

Identification of AtlA residues important for activity *in vitro*

Based on the structural analysis of the AtlA catalytic domain and the docking of a peptidoglycan fragment, we investigated the role of several residues potentially involved in substrate recognition and catalysis. These included the catalytic glutamate residue Glu246 that had not been previously studied, Lys232, Phe259, Thr312 and Tyr316. Tyr247 was added as a control, as this residue is not expected to contribute to the catalytic activity of AtlA. The expression plasmid encoding full length recombinant AtlA was mutagenized to introduce these 5 mutations in the catalytic domain. All recombinant proteins were expressed as soluble proteins and were purified by affinity chromatography (Fig. 5A). Circular dichroism confirmed that the mutations had no major impact on the overall fold of the recombinant proteins (Fig. S3). Using *M. lysodeikticus* autoclaved cells as a substrate, we determined the specific activity of individual mutants using the

spectrophotometric assay previously described (Fig. S4). The Tyr247Ser and Tyr316Ser mutations had a limited impact on *in vitro* specific activity (2.2-fold and 2.4-fold decrease, respectively) whilst the four other mutations (Lys232Ala, Phe259Val, Thr312Val and Glu246Gln) had a pronounced impact, leading to residual activities between 2.5% to 5.3% when compared to the WT enzyme (Fig. 5B).

A

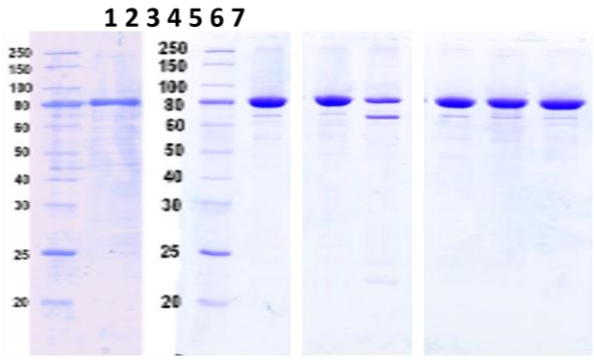

B

	Allele	Specific activity [a]	% WT
1	WT	444.6 ± 27.2	100.0
2	K232A	17.5 ± 2.3	3.9
3	Y247S	198.6 ± 55.0	44.7
4	F259V	23.4 ± 2.4	5.3
5	T312V	20.1 ± 4.1	4.5
6	Y316S	183.6 ± 17.8	41.3
7	E246Q	11.3 ± 0.8	2.5

[a] ΔOD_{450nm}/h/mg

Figure 5. Purification and characterisation of recombinant AtlA enzymatic activity. A, SDS-PAGE analysis of full length recombinant AtlA proteins. AtlA variants were produced in *E. coli* and purified using a one-step immobilized metal affinity chromatography; lane 1, WT; lane 2, K232A; lane 3, Y247S; lane 4, F259V; lane 5, T312V; lane 6, Y316S; lane 7, E246Q. **B**, specific activity (expressed as Δo_{600nm}/h/mg) was measured using *M. luteus* as a substrate.

Identification of AtlA residues important for septum cleavage

AtlA is a secreted autolysin that undergoes posttranslational modifications including proteolytic cleavage and glycosylation (4). To confirm the results obtained with recombinant proteins *in vitro*, we sought to measure the impact of mutations using cell chain length as a readout of enzymatic activity (Fig. 6). Each mutation was introduced on the chromosome by allelic exchange and the forward scattered light associated with mutant cells was measured by flow cytometry to investigate the capacity of individual AtlA mutant proteins to cleave the septum. All mutant proteins were produced at a similar level, indicating that mutations had very little (if any) impact on stability (Fig. 6A). The results were consistent with previous enzymatic assays and the docking model. Tyr247Ser has no impact on septum cleavage, confirming that the mutation does not affect the structure of the enzyme. The other five mutations had a clear impact on septum cleavage, forming cell chains significantly longer than the wild type (Fig. 6B). As expected, Glu212Gln and Glu246Gln mutations had the most pronounced impact on AtlA activity, leading to the formation of extremely long cell chains. Both Phe259 and Lys232 were shown to be critical for AtlA activity, whilst Thr312 had a relatively smaller role.

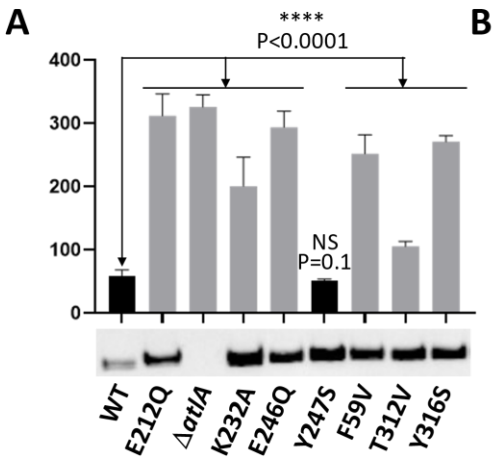

B

Strain	Median FSLog	*P* value vs Δ*atlA*	
WT	67.2 ± 2.5	<0.0001	****
E212Q	334.3 ± 24.5	0.4112	NS
Δ*atlA*	319.7 ± 22.9	NA	
K232A	204.1 ± 58.9	0.0001	***
E246Q	271.9 ± 4.2	0.0005	***
Y247S	52.8 ± 1.1	<0.0001	****
F259V	273.0 ± 22.8	<0.0001	****
T312V	112.6 ± 2.1	<0.0001	****
Y316S	278.3 ± 3.6	0.0329	*

Figure 6. Flow cytometry analysis of bacterial cell chain length in *E. faecalis* strains expressing AtlA mutant alleles. A, Median forward scattered (FSC) light of exponentially growing cells was measured by flow cytometry. The results shown correspond to the average value of six biological replicates for the parental strain (WT), the *atlA* in-frame deletion mutant (Δ*atlA*) and the six strains producing AtlA mutant alleles. All cell chain lengths were significantly different from the wild-type strain (****P<0.0001). The amount of protein produced by each strain was checked by Western blot using an anti-AtlA polyclonal serum. **B**, Median FSC values were compared to that from the Δ*atlA* mutant; NS, not significant; N/A, not applicable.

Discussion

The enzymatic assays using recombinant AtlA and measurement of septum cleavage in strains expressing AtlA variant provided insightful information to propose a catalytic mechanism. Glu212 is strictly conserved in the GH73 enzyme family and was previously identified as an essential catalytic residue (4). It is positioned at the end of helix α2, on a highly conserved α-lobe and superimposes with Glu122 from *L. monocytogenes* Auto (9), and Glu184 from $FlgJ_{St}$ (12) (Figure 1B). AtlA Glu212 can therefore be confidently identified as the catalytic proton donor. A second glutamate, Glu246, is positioned on strand β1 like Glu156 in Auto and Glu223 in $FlgJ_{St}$ (Figure 1B et D) and has been proposed to be a nucleophile/base catalyst. This second glutamate residue is conserved only in a subgroup of proteobacteria and the bacteroidetes as mentioned in the phylogenetic study that classified the GH73 sequences into 5 different clusters (10). In clusters 1 and 2, GH73 enzymes possess a β-lobe that folds into an extended β–hairpin that contributes to shaping the active site and harbours a conserved glutamate (10). This β–hairpin has been modelled in Auto, $FlgJ_{St}$, and more recently in *Sphingomonas sp.* FlgJ but is often incomplete in other structural homologs like TM0633, due to its flexibility (9,10,12,13). In Auto and $FlgJ_{St}$ structures, the position of the β-hairpin places the two catalytic glutamates at 13Å and 20Å apart respectively, and this is due to the presence of an α-helix or a β-strand of a neighbouring symmetry monomer that occludes their active sites (9,12,13) (Fig 1B)(Figure 7A).

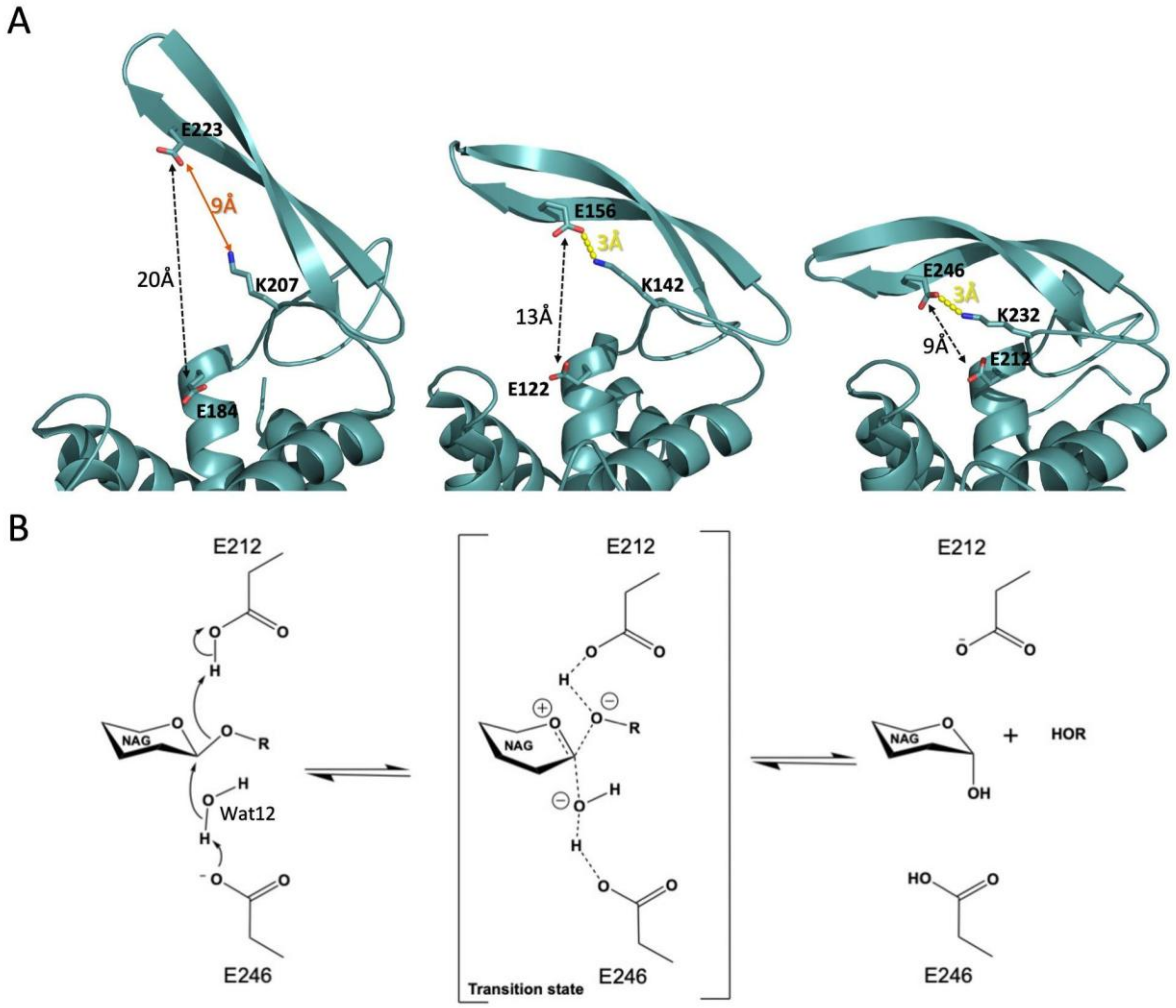

Figure 7: AtlA catalytic mechanism. **A,** The motion performed by the β-hairpin to close on the active site is shown by comparing $FlgJ_{St}$, Auto and AtlA β-hairpin's positions. In AtlA and Auto, Lys232 and Lys142 make electrostatic bonds with the nucleophiles Glu246 and Glu156 respectively (yellow dashes lines). In $FlgJ_{St}$, Lys207 is too far to bind to Glu223. **B,** AtlA is an N-acetylglucosaminidase hydrolysing the β-1,4 linkage between NAG and MurNAc using an inverting mechanism. Glu246 (catalytic base) activate a wat12 by abstracting a proton, which enable the water molecule to make a nucleophilic attack on the anomeric carbon and lead to the formation of an oxocarbenium ion-like transition state. Glu212 play the role of an acid that will donate a hydrogen to the scissile glycosidic bond. This glycolysis produces an α-anomeric configuration of the NAG at the reducing end.

In these structures, the β-hairpin is widely open, and the authors suggest that the β-hairpin takes this position to accommodate the substrate in the active site. In AtlAc, the β-hairpin shows a

"closed" conformation and the distance between Glu212 and Glu246 is 9 Å, which is the distance required for a classic type 2 nucleophile substitution with an inverting mechanism (14) (Figure 7A). We, therefore, propose that Glu212 acts as a general acid to protonate the glycosidic oxygen, favouring the aglycon departure, while the general base Glu246 activates a water molecule to make a nucleophile attack on the sugar anomeric carbon. Glu246 OE1 is making a hydrogen bond with a water molecule (Wat12) and Lys232 (Figure 7B). This water molecule could therefore be activated by Glu246 if the latter encounters a displacement of a negative charge and takes a proton from Wat12, which will, in turn, be able to perform the nucleophilic attack on the anomeric carbon of the substrate. In previous studies where structural homologs show a β-hairpin widely open, the authors proposed that the β-hairpin will undergo several conformational changes to accommodate the substrate in the active site and subsequently place the two catalytic glutamate residues at the proper distance for hydrolysis of the glycosidic bond (14). Our crystallographic data strongly support this model and suggest a contribution of a conserved lysine residue (Lys232) in this process, as demonstrated by the loss of AtlA activity associated with the Lys232 mutation both *in vitro* and *in vivo*. The structure of Auto illustrates an intermediary position of the β -hairpin where the Lys142 can reach the catalytic Glu and make electrostatic contact to initiate the closing of the β -hairpin. Our AtlAc crystal structure shows the electrostatic bond between Lys232 and Glu246 maintaining the position of the β-hairpin resulting in a closed active site (Figure 7A). We propose that this electrostatic contact between the Lys232 and the Glu246 stabilizes the charges to help its attack on the water molecule. The identification of the endoglucosaminidase activity together with modelling of the tetrasaccharide peptide bound in the active site indicates that after the movement of the β-hairpin, Lys232 adopts another conformation to allow substrate binding and catalysis using an inverting mechanism.

Collectively, our results indicate that AtlA uses an inverting mechanism to hydrolyse the β-1,4 glycosidic bond.

Experimental procedures

Bacterial strains, plasmids, and growth conditions. All strains and plasmids used in this study are described in Table S1. The bacteria were grown at 37°C in Brain Heart Infusion broth or agar (15 g/l) (BHI, Difco laboratories, Detroit, USA). When required, *E. coli* was grown in the presence of 100 µg/ml ampicillin (for protein expression) or 200 µg/ml erythromycin (for pGhost selection). *E. faecalis* transformants were selected with 30 µg/ml erythromycin.

Plasmid construction. pML420 was built to express AtlA catalytic domain. The DNA fragment encoding amino acids 172 to 337 was PCR amplified from V583 genomic DNA (15) with oligonucleotides EF Atla_cat_F and Atla_cat_R (Table S1) using Vent DNA polymerase (NEB). The resulting fragment was cloned in frame with the hexahistidine sequence of pET2818, a pET2816b derivative (8), using NcoI and BamHI. Plasmids expressing full-length AtlA derivatives (with single amino-acid substitutions) were constructed by site-directed mutagenesis using plasmid pML118 as a template (8) following the quickchange mutagenesis protocol (16) and oligonucleotides described in Table S1. pML118 derivatives were used as a template to amplify the DNA fragments encoding atlA alleles. The corresponding PCR products were cloned in pGhost9 using XhoI and EcoRI.

Construction of *E. faecalis* mutants by allele exchange. The protocol described previously was followed (17). *E. faecalis* was electroporated with pGhost9 derivatives and transformants were selected at 30°C in the presence of erythromycin. Single crossing-overs were induced at non-permissive temperature (42°C) and screened by PCR. The second recombination event was triggered by subculturing recombinant clones in BHI at 42°C. Erythromycin sensitive colonies were screened by PCR to identify mutants.

Production and purification of recombinant proteins.

E. coli Rosetta(DE3) pLysS cells (Novagen) containing recombinant pET vectors were cultured in ZY auto-induction medium (18) containing 100 mg/ml of ampicillin and 34 mg/ml of chloramphenicol at 37 °C until the OD600 reaches 0.6. The cultures were then incubated overnight at 17 °C. Cells were harvested by centrifugation and the frozen pellets were resuspended in lysis buffer (50 mM Tris-HCl pH 8, 300 mM NaCl, 10 mM imidazole, 1mM EDTA, 0.25 mg/ml Lysozyme, 5% glycerol, 0.1% triton). After a 30 min incubation with 0.1 mg/ml deoxyribonuclease and 0.02M magnesium sulphate at 4°C, the cells were disrupted by sonication on ice. The lysate was clarified by centrifugation and the supernatant was applied onto a nickel-chelate affinity resin using an ÄktaXpress (Cytiva). The resin was washed with 50 mM Tris-HCl pH 8, 300 mM NaCl, and 50 mM imidazole. The protein was eluted with 50 mM Tris-HCl pH 8, 300 mM NaCl, and 250 mM imidazole and dialyzed against the gel filtration buffer (20 mM Mes pH 6, 100 mM NaCl and 1mM DTT). The protein was further purified on a Superdex 75 16/60 column (Cytiva). Pure fractions, as analyzed by SDS-PAGE, were pooled.

Circular Dichroism Spectroscopy

CD samples were diluted to a concentration of 0.25mg/ml in 25 mM Tris-HCL + 150mM NaCl buffer, pH 8.0. Far-UV CD spectra were acquired with a Jasco J-810 spectropolarimeter using a 0.1 cm pathlength cell. Spectra were acquired with a Peltier thermally controlled cuvette holder at 25°C, from 190 to 350 nm, with a data pitch of 1 nm at a rate of 50 nm/min, a response time of 8 seconds and averaged over 5 accumulations. Mean residue ellipticity, $[\Theta]_{MRW}$ (deg cm^2 $dmol^{-1}$) was calculated to allow reliable comparison of different proteins using the equation:

$$[\Theta]_{MRW} = \frac{(\Theta \times 100 \times M_r)}{(c \times d \times N_A)}$$

where Θ is the measured ellipticity in degrees, M_r is the protein molecular weight in kDa, c is the protein concentration in mg/ml, d is the pathlength in centimetres, N_A is the number of amino acids per protein. The factor of 100 converts molar concentration to dmol/cm^3 (19).

Crystallization, data collection and processing

The catalytic domain of AtlA (AtlAc) was concentrated to 14 mg/ml using a 10 kDa cut-off ultracentrifugation membrane (Thermoscientific). Crystals were obtained at 20°C by screening The Wizard Classic crystallization kit (Molecular Dimensions™) using a nanoliter sitting drops setup with automated crystallization TECAN Genesis and ttplabtech Mosquito robots. A total of 300 µl of AtlAc (14 mg ml/1) was mixed to 100 µl of reservoir solution composed of 0.2 M Magnesium chloride, 10% polyethylene glycol (PEG) 3000 and 0.1M Na-Cacodylate pH 6.5. A single crystal of AtlAc was mounted on a rayon loop, soaked in a cryoprotectant solution composed of the crystallization conditions with 23% glycerol and subsequently flash-cooled to 120 K. A data set was collected at 1.4 Å at the ID30B beamline (ESRF, France). Data were integrated, scaled and reduced with XDS (20) and AIMLESS (21). Unless otherwise cited, all further crystallographic computations were carried out using the CCP4 suite of programmes (21).

Phasing, Model Building, and Refinement

The structure was solved by molecular replacement, using MolRep (22), with a search model of AtlAc built by Modeller using Auto structure from *L. monocytogenes* (54% sequence identity with AtlAc) as a template (PDB 3fi7) (9,23). The solution of MolRep gave a correlation coefficient of 0.47 for one monomer in the asymmetric unit. The electron density map calculated from the model was of sufficient quality to allow tracing of 99% of the molecule (156 residues) using the REFMAC/ARP-wARP programs (24,25). Unless otherwise cited, all further crystallographic computations were carried out using the CCP4 suite of programs (21). The

model was refined using REFMAC (24) with manual correction using Coot (26). The final model contains 1281 non-hydrogen protein atoms with 182 water molecules and 5 glycerol molecules. The crystallographic *R*cryst and *R*free values are 14 and 17%, respectively (see Table 1).

Docking experiments

Molecular docking was performed in Autodock Vina (27). The structure of Atla was used as a docking model. Ligand and receptor structures were prepared in Jligand (28) and AutoDockTools (29). Partial charges were calculated using Gasteiger-Hückel method. Exhaustiveness was set to 8 and default parameters were used unless otherwise stated. The ligand was treated as flexible, and the protein was kept rigid during the docking runs, except for the side chain of Lys232, which was treated as flexible. The grid size was set to 22 x 30 x 24 (Å) and the grid box's center points were set to target the active site of the protein, with the center at X = 32, Y = 20, Z = -11.5. All 3D and 2D representations of protein-ligand complexes were visualized using PyMOL (The PyMOL Molecular Graphics System, Schrödinger, LLC) and Ligplot+ (30), respectively.

Determination of peptidoglycan hydrolase activity.

Hydrolysis of purified cell walls was measured using an Ultrospec 2000 spectrophotometer (Amersham biosciences, Uppsala, Sweden) and following the decrease in turbidity at 450 nm for 15 min at 37°C in 25 mM Tris-HCl, pH 7.5, 100 mM NaCl buffer. Peptidoglycan was resuspended at a concentration giving an absorbance at 450nm of 0.6. Various dilutions of AtlA and its derivatives were tested to identify conditions in which the velocity of hydrolysis was proportional to enzyme concentration. Enzymatic activity was expressed as A_{450} units per min per mmol of protein; the residual activity of individual mutants was expressed as the percentage of wild-type activity.

For zymogram analysis, crude extracts were separated by SDS-PAGE using gels containing 0.2 % autoclaved *Micrococcus lysodeikticus* cells. After electrophoresis, the proteins were renatured by incubating the gel for 24 h in 25 mM Tris (pH 8.0) buffer containing 0.1 %Triton at 37°C. Lytic activities could be visualized as clear bands on the opaque SDS-PAGE.

Western blot analyses

Cells were grown in BHI to exponential phase. The equivalent of 250µl of acid-washed <106µm glass beads (SIGMA) was added to a 1.5ml aliquot of the culture and cells were broken using a Fastprep homogenizer (MP Biomedicals) with 6 cycles at maximum speed with 1 min pause between cycles. The equivalent of 25µl of culture was loaded on a 12% SDS-PAGE and transferred to nitrocellulose. AtlA was detected using a rabbit polyclonal antibody against the full-length protein as previously described (4).

Flow cytometry and statistical analyses

Overnight static cultures at 37°C were diluted 1:100 into fresh broth (OD600 ~0.02) and grown to mid-exponential phase (OD600~0.2 to 0.4). Bacteria were diluted 1:100 in filtered phosphate buffer saline and analyzed by flow cytometry using a Millipore Guava easyCyte H2L system. Light scatter data were obtained with logarithmic amplifiers for 20,000 events. Forward scattered light values were compared using Graphpad and an unpaired t test with Welch's correction.

Table 1 Structural data collection and refinement statistics

Crystal parameters	
Space group	$P3_121$
Cell parameters (Å)	a=b=62.55, c=93.22
Data quality	
Wavelength (Å)	0.9762 (PX1)
Resolution of data (Å)	46.8-1.45
Unique reflections	38042
R_{merge} (outer shell)	0.06 (0.93)
Mean *I/I* (outer shell)	9.8 (1.1)
Completeness (outer shell) %	99.9 (99.9)
CC1/2 (outer shell)	0.99 (0.76)
Multiplicity (outer shell)	4.7 (4.2)
Refinement	
R_{cryst} [b]	0.14
R_{free} [c]	0.17
Root mean square deviation 1-2 bonds (Å)	0.012
Root mean square deviation 1-3 angles (°)	1.539

[a] $R_{\text{merge}} = (S_{hkl}\, S_i ½ I_{hkl} - (I_{hkl})½ / S_{hkl}\, S_i\, [I_{hkl}])$.
[b] $R_{\text{cryst}} = S_{\text{hkl}} |Fo| - |Fc| / S_{\text{hkl}} |Fo|$
[c] R_{free} is calculated for randomly selected reflections excluded from refinement

Data availability

All data presented in this article are to be shared upon request to Dr Florence Vincent (fvincent.cnrs@univ-amu.fr) or Dr Stéphane Mesnage (s.mesnage@sheffield.ac.uk).

The atomic coordinates of AtlAc were deposited in the PDB (entry 7QFU)

Supporting information

This article contains supporting information (Figures S1, S2, S3, S4 and Table S1).

Acknowledgments

This work was supported by an International Exchange grant from the Royal Society to SM and FV (IEC\R2\170260).

Author contributions

Conceptualization: SM and FV; Data curation: SB, SM and FV; Formal Analysis: SB, NG, SM and FV; Funding acquisition: SM and FV; Investigation: VZ, SB, RD, NG, AG, PN, CG, BS, PJD, SM and FV ; Methodology: SB and FV; Project administration: SM and FV; Supervision: SM and FV ; Validation : VZ, SB, NG, BS, SM and FV ; Visualization: SB, SM and FV ; Writing – original draft: SM and FV ; Writing – review & editing : SB, SM and FV.

References

1. Arias, C. A., and Murray, B. E. (2012) The rise of the *Enterococcus*: beyond vancomycin resistance. *Nat Rev Microbiol* **10**, 266-278

2. Bradley, C. R., and Fraise, A. P. (1996) Heat and chemical resistance of enterococci. *J Hosp Infect* **34**, 191-196

3. Ramos, Y., Sansone, S., and Morales, D. K. (2021) Sugarcoating it: Enterococcal polysaccharides as key modulators of host-pathogen interactions. *PLoS Pathog* **17**, e1009822

4. Salamaga, B., Prajsnar, T. K., Jareno-Martinez, A., Willemse, J., Bewley, M. A., Chau, F., Ben Belkacem, T., Meijer, A. H., Dockrell, D. H., Renshaw, S. A., and Mesnage, S. (2017) Bacterial size matters: Multiple mechanisms controlling septum cleavage and diplococcus formation are critical for the virulence of the opportunistic pathogen *Enterococcus faecalis*. *PLoS Pathog* **13**, e1006526

5. Bravetti, A. L., Mesnage, S., Lefort, A., Chau, F., Eckert, C., Garry, L., Arthur, M., and Fantin, B. (2009) Contribution of the autolysin AtlA to the bactericidal activity of amoxicillin against *Enterococcus faecalis* JH2-2. *Antimicrob Agents Chemother* **53**, 1667-1669

6. Dubee, V., Chau, F., Arthur, M., Garry, L., Benadda, S., Mesnage, S., Lefort, A., and Fantin, B. (2011) The *in vitro* contribution of autolysins to bacterial killing elicited by amoxicillin increases with inoculum size in *Enterococcus faecalis*. *Antimicrob Agents Chemother* **55**, 910-912

7. Drula, E., Garron, M. L., Dogan, S., Lombard, V., Henrissat, B., and Terrapon, N. (2022) The carbohydrate-active enzyme database: functions and literature. *Nucleic Acids Res* **50**, D571-D577

8. Eckert, C., Lecerf, M., Dubost, L., Arthur, M., and Mesnage, S. (2006) Functional analysis of AtlA, the major *N*-acetylglucosaminidase of *Enterococcus faecalis*. *J Bacteriol* **188**, 8513-8519

9. Bublitz, M., Polle, L., Holland, C., Heinz, D. W., Nimtz, M., and Schubert, W. D. (2009) Structural basis for autoinhibition and activation of Auto, a virulence-associated peptidoglycan hydrolase of *Listeria monocytogenes*. *Mol Microbiol* **71**, 1509-1522

10. Lipski, A., Herve, M., Lombard, V., Nurizzo, D., Mengin-Lecreulx, D., Bourne, Y., and Vincent, F. (2015) Structural and biochemical characterization of the beta-N-acetylglucosaminidase from *Thermotoga maritima:* toward rationalization of mechanistic knowledge in the GH73 family. *Glycobiology* **25**, 319-330

11. Taly, J. F., Magis, C., Bussotti, G., Chang, J. M., Di Tommaso, P., Erb, I., Espinosa-Carrasco, J., Kemena, C., and Notredame, C. (2011) Using the T-Coffee package to build multiple sequence alignments of protein, RNA, DNA sequences and 3D structures. *Nat Protoc* **6**, 1669-1682

12. Zaloba, P., Bailey-Elkin, B. A., Derksen, M., and Mark, B. L. (2016) Structural and Biochemical insights into the peptidoglycan hydrolase domain of FlgJ from *Salmonella typhimurium*. *PLoS One* **11**, e0149204

13. Hashimoto, W., Ochiai, A., Momma, K., Itoh, T., Mikami, B., Maruyama, Y., and Murata, K. (2009) Crystal structure of the glycosidase family 73 peptidoglycan hydrolase FlgJ. *Biochem Biophys Res Commun* **381**, 16-21

14. McCarter, J. D., and Withers, S. G. (1994) Mechanisms of enzymatic glycoside hydrolysis. *Curr Opin Struct Biol* **4**, 885-892

15. Paulsen, I. T., Banerjei, L., Myers, G. S., Nelson, K. E., Seshadri, R., Read, T. D., Fouts, D. E., Eisen, J. A., Gill, S. R., Heidelberg, J. F., Tettelin, H., Dodson, R. J., Umayam, L., Brinkac, L., Beanan, M., Daugherty, S., DeBoy, R. T., Durkin, S., Kolonay, J., Madupu, R., Nelson, W., Vamathevan, J., Tran, B., Upton, J., Hansen, T., Shetty, J., Khouri, H., Utterback, T., Radune, D., Ketchum, K. A., Dougherty, B. A., and Fraser, C. M. (2003) Role of mobile DNA in the evolution of vancomycin-resistant *Enterococcus faecalis*. *Science* **299**, 2071-2074

16. Liu, H., and Naismith, J. H. (2008) An efficient one-step site-directed deletion, insertion, single and multiple-site plasmid mutagenesis protocol. *BMC Biotechnol* **8**, 91

17. Mesnage, S., Chau, F., Dubost, L., and Arthur, M. (2008) Role of *N*-acetylglucosaminidase and *N*-acetylmuramidase activities in *Enterococcus faecalis* peptidoglycan metabolism. *The Journal of biological chemistry* **283**, 19845-19853

18. Grabski, A., Mehler, M., and Drott, D. (2005) The overnight express autoinduction system: high-density cell growth and protein expression while you sleep. *Nature methods* **2**, 233-235

19. Creighton, T. E. (1989) *Protein structure: a practical approach*, Oxford University Press

20. Kabsch, W. (2010) Xds. *Acta Crystallogr D Biol Crystallogr* **66**, 125-132

21. Dodson, E. J., Winn, M., and Ralph, A. (1997) Collaborative Computational Project, number 4: providing programs for protein crystallography. *Methods Enzymol* **277**, 620-633

22. Vagin, A., and Teplyakov, A. (2010) Molecular replacement with MOLREP. *Acta Crystallogr D Biol Crystallogr* **66**, 22-25

23. Webb, B., and Sali, C. (2016) *Comparative protein structure modeling using Modeller*, John Wiley & Sons, Inc.

24. Murshudov, G. N., Vagin, A. A., and Dodson, E. J. (1997) Refinement of macromolecular structures by the maximum-likelihood method. *Acta Crystallogr D Biol Crystallogr* **53**, 240-255

25. Perrakis, A., Harkiolaki, M., Wilson, K. S., and Lamzin, V. S. (2001) ARP/wARP and molecular replacement. *Acta Crystallogr D Biol Crystallogr* **57**, 1445-1450

26. Emsley, P., and Cowtan, K. (2004) Coot: model-building tools for molecular graphics. *Acta Crystallogr D Biol Crystallogr* **60**, 2126-2132

27. Trott, O., and Olson, A. J. (2010) AutoDock Vina: improving the speed and accuracy of docking with a new scoring function, efficient optimization, and multithreading. *J Comput Chem* **31**, 455-461

28. Lebedev, A. A., Young, P., Isupov, M. N., Moroz, O. V., Vagin, A. A., and Murshudov, G. N. (2012) JLigand: a graphical tool for the CCP4 template-restraint library. *Acta Crystallogr D Biol Crystallogr* **68**, 431-440

29. Morris, G. M., Huey, R., Lindstrom, W., Sanner, M. F., Belew, R. K., Goodsell, D. S., and Olson, A. J. (2009) AutoDock4 and AutoDockTools4: Automated docking with selective receptor flexibility. *J Comput Chem* **30**, 2785-2791

30. Laskowski, R. A., and Swindells, M. B. (2011) LigPlot+: multiple ligand-protein interaction diagrams for drug discovery. *J Chem Inf Model* **51**, 2778-2786